Carbohydrate Polymers 89 (2012) 7–16

Contents lists available at SciVerse ScienceDirect

Carbohydrate Polymers

journal homepage: www.elsevier.com/locate/carbpol

Theoretical and experimental investigation on dissolution and regeneration of cellulose in ionic liquid

Zhen-Dong Ding, Zhen Chi, Wen-Xiu Gu*, Sheng-Ming Gu, Jian-Hua Liu, Hai-Jun Wang*

School of Chemical and Material Engineering, Jiangnan University, Wuxi, Jiangsu 214122, China

ARTICLE INFO

Article history:
Received 16 December 2011
Received in revised form 24 January 2012
Accepted 26 January 2012
Available online 3 February 2012

Keywords:
Cellulose
Ionic liquid
Dissolution
Regeneration

ABSTRACT

Density functional theory calculations and atoms in molecules theory were performed to investigate the mechanism of cellulose dissolution and regeneration in 1-ethyl-3-methylimidazolium acetate ([emim]Ac), and (1,4)-dimethoxy-β-D-glucose (Glc) was chosen as the model for cellulose. The theoretical results show that the interaction of [emim]Ac with Glc is stronger than that of Glc with Glc. Further studies indicate that the anion acetate of [emim]Ac forms strong H-bonds with hydroxyl groups of Glc. It is also observed that the H-bonds between [emim]Ac and Glc are weakened or even destroyed by the addition of water. In addition, both the original and regenerated cellulose samples were characterized with FT-IR, XRD, TGA and SEM. The experimental results prove that cellulose can be readily reconstituted from the [emim]Ac-based cellulose solution by the addition of water and the crystalline structure of cellulose is converted to cellulose II from cellulose I in the original cellulose.

1. Introduction

Cellulose is the most abundant biorenewable material, with a long and well-established technological base (Kirk-Othmer, 1993), and has a highly crystalline polymer of D-an-hydroglucopyranose units joined together in long chains by β-1,4-glycosidic bonds (Li & Zhao, 2007). The derived products of cellulose have many important applications in the fiber, paper, membrane, polymer and paint industries. The growing willingness to develop new cellulosic materials results from the fact that cellulose is a renewable resource. Although many of the technologies currently used in cellulose processing are decidedly nongreen (Johnson et al., 1985), it is practically difficult to dissolve cellulose in most common organic solvents, because of their stiff molecules and closed chain packing via numerous intermolecular and intramolecular H-bonds (Zhang, Wu, Zhang, & He, 2005). Recently, various types of solvents have been used for dissolving of cellulose. For example, dimethylacetamide/lithium chloride, N_2O_4-N, *N*-dimethylformamide, $LiClO_4{\cdot}3H_2O$, $LiSCN{\cdot}2H_2O$ and *N*-methyl-morpholine-*N*-oxide/H_2O system (Li & Zhao, 2007; Song, Wang, & Xing, 2009; Tan et al., 2009; Zhang et al., 2005). However, these solvents have some limitations such as volatility, toxicity, difficulty for solvent recovery and instability in application. The *N*-methylmorpholine-*N*-oxide/H_2O system is the only one industrialized for manufacturing regenerated cellulose. However, it has some disadvantages such as the demand for high temperature to dissolve and high cost (Tan et al., 2009). Therefore, better cellulose solvents are key to taking greater advantage of cellulose.

Ionic liquids (ILs) have been used for many aspects, ranging from media for organic synthesis and catalysts to lubricants, and more recently have generated much academic interest as replacements for environmentally damaging volatile organic solvents (Berg, Deetlefs, Seddon, Shim, & Thompson, 2005). The appearance of ILs provides a broader scope for the development of cellulose chemistry. ILs have been proven as the efficient solvents for cellulose dissolution because of their unique properties, such as low melting points, negligible vapor pressure, nonvolatile and inflammable as well as wide electrochemical windows (Huddleston et al., 2001). It has been found that cellulose can be dissolved without derivatization in high concentrations using ILs. Such as 1-allyl-3-methylimidazoliumchloride, 1-allyl-3-methylimidazolium formate, 1-butyl-3-methylimidazolium chloride and so on (Fu, Mazza, & Tamaki, 2010). Furthermore, the components of cation and anion in the ILs can be fine-tuned to adjust the physicochemical properties, which affect their performance in the interaction with the cellulose.

NMR experiments, DFT calculations and molecular mechanics simulations have provided mechanistic insight into cellulose dissolution in IL. Zhang et al. (2005) speculated that the possible dissolution mechanism of cellulose in 1-allyl-3-methylimidazolium chloride is that Cl^- ions associated with the cellulose hydroxyl proton, and the free cations complex with the cellulose hydroxyl oxygen, which disrupted H-bonds in cellulose and led to the

* Corresponding authors.
E-mail addresses: wenxiugu@gmail.com (W.-X. Gu), wanghj329@hotmail.com (H.-J. Wang).

0144-8617/$ – see front matter © 2012 Elsevier Ltd. All rights reserved.
doi:10.1016/j.carbpol.2012.01.080

dissolution of cellulose. Remsing, Swatloski, Rogers, and Moyna (2006) demonstrated that the solution of cellulose by 1-*n*-butyl-3-methylimidazolium chloride involves H-bonds between the carbohydrate hydroxyl and chloride ions. Youngs, Hardacre, and Holbrey (2007) indicated that dominant contributions to the sugar–ionic liquid interaction energy come from favorable H-bond interactions between hydroxyls and chlorides. Guo, Zhang, Duan, and Liu (2010) applied density functional theory calculations to investigate the interactions of the cellulose molecule with several anions, and found that the strength of interactions of anions with cellulose follows the order: acetate anion > alkylphosphate anion > tetrafluoroborate anion > hexafluorophosphate anion. Janesko applied dispersion-corrected density functional theory to study the differences between ionic liquids' interactions with cellulose vs. lignin, and emphasized that cellulose preferentially interacts with Cl^- (Janesko, 2011). Up to now, there are no DFT calculations and AIM theory analyses concerning the dissolution and regeneration mechanism of cellulose in [emim]Ac. In this paper, Glc was chosen as the model of cellulose to investigate the interaction between [emim]Ac and cellulose at the molecular level. In addition, the reconstitution of cellulose from [emim]Ac-based cellulose solution by the addition of water has been demonstrated by theoretical and experimental research. The regenerated cellulose was characterized by FT-IR, XRD, TGA and SEM compared with the original cellulose. We hope that these efforts will result in better understanding of the dissolution of cellulose in ILs.

2. Materials and methods

2.1. Materials

N-methylimidazole was obtained from Changzhou Chemical Factory and further purified by distillation. Bromoethane and ethyl acetate were distilled and then were stored over molecular sieves in tightly sealed glass bottles, respectively. Other chemicals (AR) were commercially available and were used without further purification.

2.2. Quantum chemical calculations methods

All energy minimization calculations were performed with Gaussian 03, and the AIM calculations were performed with the AIM2000 package (Frisch et al., 2003). The hybrid Becke 3–Lee–Yang–Parr (B3LYP) exchange-correlation function with the 6-31+G* basis set was employed to perform the geometry optimizations in this work (Bader, 1990; Lee, Yang, & Parr, 1988). The B3LYP/6-31+G* level represents an excellent trade-off between accuracy and computer requirements, particularly suitable for the investigation of ionic liquid and cellulose system (Guo, Zhang, & Liu, 2010).

2.3. Preparation of [emim]Ac

[emim]Ac was prepared following the reported procedures (Ellis, 1996; Yang, Zhang, Wang, & Tong, 2006). [emim]Br was synthesized by refluxing the *N*-methylimidazole with excess bromoethane at 50 °C for 48 h. The excess bromoethane was removed by evaporation and the crude product was recrystallized twice by ethyl acetate. The resulting precipitate was brownish and was dried in vacuum for 24 h under reduced pressure. Then 0.2 mol [emim]Br and 0.1 mol $Pb(Ac)_2{\cdot}3H_2O$ were separately dissolved in solutions of methanol–water (4:1 v/v). Upon mixing the two solutions, a precipitate of $PbBr_2$ was produced, which was removed by filtration after cooling at −20 °C overnight. The solvent was removed from the filtrate by rotary evaporation, and the product [emim]Ac was gotted by drying in vacuum for 2 days at 80 °C. The structure of [emim]Ac was confirmed by ^{1}H NMR (400 MHz, D_2O): δ_H = 1.46–1.52 (t, 3 H; CH_3), δ_H = 1.89–1.94 (t, 3 H; CH_3—COO^-), δ_H = 3.89 (t, 3H; N—CH_3), δ_H = 4.18–4.26 (t, 2H; CH_2), δ_H = 7.4 (s, 1H; Ring-CH), δ_H = 7.5 (s, 1H; Ring-CH), δ_H = 8.7 (s, 1H; Ring-CH).

2.4. Cellulose dissolution and regeneration experiments

The dissolution of microcrystalline cellulose (MCC) was carried out in a round bottom flask that was heated in the oil-bath with vigorous magnetic stirring in the open atmosphere. 0.50 g of MCC was added to 10 g of [emim]Ac in a 25 mL beaker (Sun et al., 2009). When the color of the solution turns amber, MCC was completely dissolved. Finally, a transparent solution with about 5% polymer concentration was obtained. Cellulose was reconstituted from the resulting clear, amber-colored, viscous liquor as flocs by rapid mixing with distilled water. The powdery off-white solids were then filtered, washed with distilled water and dried in a vacuum oven at 60 °C prior to their use in FT-IR, XRD, TGA and SEM experiments. The recovery of [emim]Ac was accomplished by evaporating to remove water.

2.5. Characterization of the original and regenerated cellulose

The original and regenerated cellulose were characterized by FT-IR using a Perkin Elmer Spectrum 100 FT-IR spectrometer equipped with an attenuated total reflectance (ATR) cell with 32 scans at 2 cm^{-1} resolution.

The original and regenerated cellulose samples were also characterized by wide-angle X-ray diffraction patterns. The X-ray diffraction patterns with Cu Kα radiation (λ = 1.5406 Å) at 40 kV and 30 mA were recorded in the range of 2θ = 5–40° with an X-ray diffraction diffractometer (D/MAX-2500, Rigaku Denki, Japan).

Differences in morphology before and after [emim]Ac treatment were analyzed by scanning electron microscopy (SEM). SEM images were taken at 2000× magnification using a Hitachi S-4800 field emission SEM instrument operated at 2 kV accelerating voltage.

The thermal decomposition curves of the original and regenerated cellulose were determined using a precisa TGA/DSC 1/1100 SF thermogravimetric analyzer. Each sample was analyzed in a platinum pan with nitrogen as the purge gas. In all experiments, the temperature was increased from 25 to 600 °C at a constant rate of 20 °C min^{-1}.

3. Results and discussion

3.1. Theoretical study of dissolution and regeneration of cellulose

3.1.1. Geometries optimization

Conformational searches were performed as follows. A series of geometric conformations of [emim]Ac, Glc, Glc–Glc, [emim]Ac–Glc [emim]Ac–$n$$H_2O$ (n = 1, 2, 3) and [emim]Ac–Glc–$n$$H_2O$ (n = 1, 2) were originally optimized at B3LYP/6-31+G* level. Geometries optimization used tight convergence criteria and no restriction on symmetries was imposed on the initial geometric conformations, therefore the geometries optimization for the saddle points occurred with all degrees of freedom. Followed by frequency calculations to verify the reasonability of the optimized structures at the corresponding level, vibration frequency analysis on these optimized structures gave no imaginary frequencies, suggesting that they are true minimum energy structures. The representative optimized configurations of [emim]Ac, Glc, Glc–Glc, [emim]Ac–Glc [emim]Ac–$n$$H_2O$ (n = 1, 2, 3) and [emim]Ac–Glc–$n$$H_2O$ (n = 1, 2) were chosen and listed in Figs. 1–3.

3.1.2. Intermolecular interaction and AIM analysis

The optimized configurations were used to characterize the preferred interaction sites, when we studied the interaction energies of Glc–Glc, [emim]Ac–Glc [emim]Ac–nH$_2$O (n = 1, 2, 3) and [emim]Ac–Glc–nH$_2$O (n = 1, 2). The interaction energy ΔE can be calculated by the use of Eq. (1):

$$\Delta E_{(\mathrm{kJ\ mol^{-1}})} = 2625.5\ \ [E_{\mathrm{AB(a.u.)}} - (E_{\mathrm{A(a.u.)}} + E_{\mathrm{B(a.u.)}})] \quad (1)$$

where E_{AB} is the total energy of the system and ($E_A + E_B$) is the sum of the energy of the pure compositions.

The interaction energy is corrected by BSSE (basis set superposition error) and ZPE (the zero point energy). Thus, the corrected interaction energy $\Delta E_{ZPE+BSSE}$ can be calculated from Eq. (2):

$$\Delta E_{\mathrm{ZPE+BSSE}} = \Delta E + \Delta E_{\mathrm{BSSE}} + \Delta E_{\mathrm{ZPE}} \quad (2)$$

where ΔE_{BSSE} is the correction of BSSE, and ΔE_{ZPE} is the correction of ZPE.

In order to obtain more information about the intermolecular interaction, the AIM theory was used to analyze the bonding characteristic (Bader, 1998). The AIM theory, based on a topological analysis of electron density (ρ_c) and laplacian ($\nabla^2\rho_c$) (Frisch

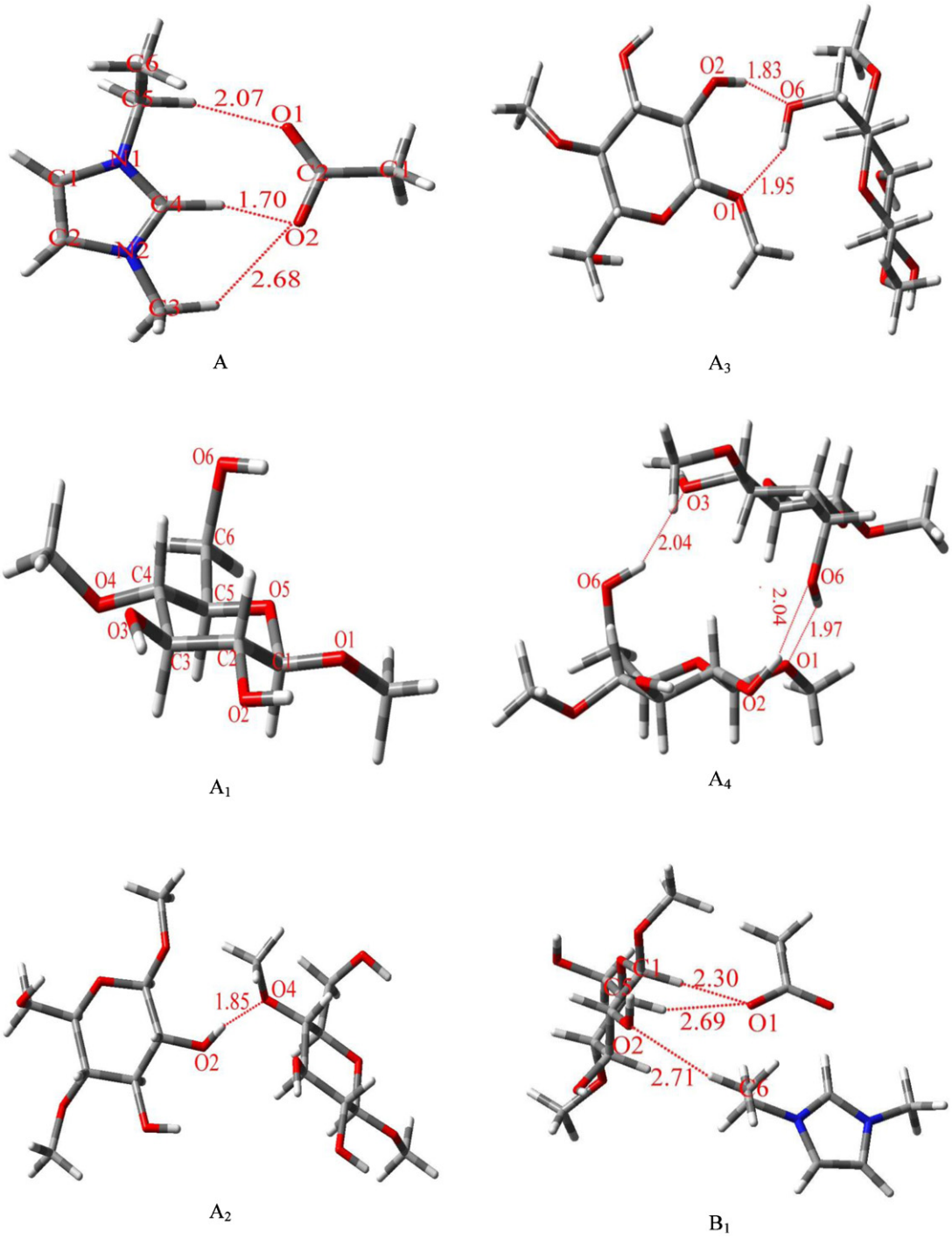

Fig. 1. The optimized configurations for [emim]Ac (A), Glc (A_1), Glc-Glc (A_{2-4}) and [emim]Ac-Glc (B_{1-3}) calculated at the B3LYP/6-31+G* level. H-bonds are indicated by dotted line, and bond lengths are in angstrom (Å).

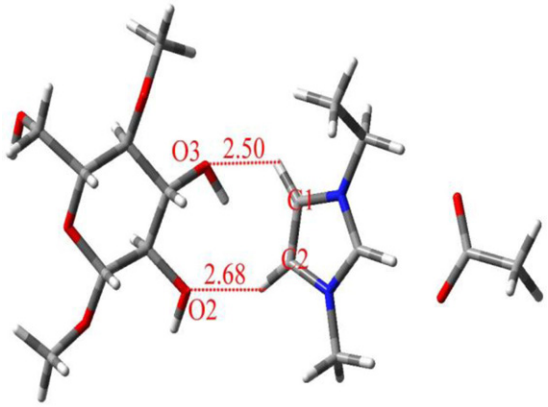

B_2

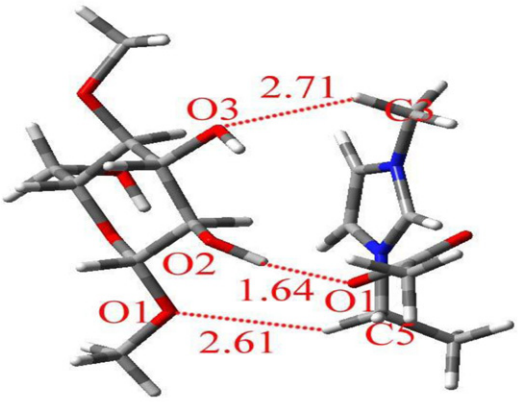

B_3

Fig. 1. (*Continued.*)

et al., 2003), provides a universally applicable tool for the classification of the bonding interactions that take place in any molecular system, even inside a supermolecule. The ρ_c is used to describe the strength of a bond, with stronger bond associated with larger ρ_c value. The $\nabla^2\rho_c$ describes the characteristic of the bond. As $\nabla^2\rho_c < 0$, it is named as the covalent bond. As $\nabla^2\rho_c > 0$, it refers to a closed-shell interaction (Solimannejad, Alkorta, & Elguero, 2007) and characteristic of ionic bond, H-bond, or van der Waals interaction. In this paper, we are only concerned with the values of ρ_c and $\nabla^2\rho_c$ for intermolecular H-bonds. There are a set of criteria for ρ_c and $\nabla^2\rho_c$ proposed at bond critical points (BCPs) for the conventional H-bonds. Both parameters for closed-shell interactions as H-bonds are positive within the following ranges: 0.002–0.035 a.u. for the electron density and 0.024–0.139 a.u. for its Laplacian (Parr & Yang, 1994).

The AIM analysis results of [emim]Ac are listed in Table 1. For most H-bonds considered here, the ρ_c and $\nabla^2\rho_c$ values lie in the relative proposed ranges. Therefore, for the observed [emim]Ac, ρ_c and $\nabla^2\rho_c$ at BCPs of H-bonds fall within 0.002–0.051 a.u. and 0.010–0.148 a.u., respectively. It can be concluded that the interactions between cation and anion which are marked by the dotted line are all closed shell system (van der Waals or H-bond interactions).

Table 1
Properties of the electron density of bond critical point for the interaction of $[emim]^+$ with Ac^- (a.u).

Bond	ρ_{BCP}	$\Delta^2\rho_{BCP}$
C5—H. . .O1	0.0217	0.0681
C4—H. . .O2	0.0508	0.1477
C3—H. . .O2	0.0058	0.0239

The H···O distances vary from 1.70 to 2.68 Å, which are longer than the corresponding covalent bond distance and shorter than the sum of the van der waals H···O distance (Bondi, 1964), indicating that H-bonds have been formed. The three H-bonds between $[enim]^+$ and Ac^- have corresponding bond lengths and angles of O_{22}—H_{10}: 2.68 Å; O_{22}—H_{13}: 1.70 Å; O_{23}—H_{15}:2.07 Å; $\angle C_1$—H_{10}—O_{22}: 138.78°; $\angle C_4$—H_{13}—O_{22}: 166.23°; $\angle C_7$—H_{15}—O_{23}: 161.89°). The results also show that the intensity of the H-bond between anion and C_4—H is stronger than the other H-bonds. Because the ρ_c is a measure of the intensity of the interaction, stronger H-bonds have greater ρ_c values and the corresponding bond length is shorter.

The intermolecular interaction energies and AIM analysis results of Glc–Glc are listed in Table 2. The ρ_c and $\nabla^2\rho_c$ at BCPs of H-bonds fall within 0.002–0.035 a.u. and 0.024–0.139 a.u., respectively. It is observed that Glc connects with each other by H-bonds. The configuration A_4 has the biggest absolute value of interaction energy (37.93 kJ/mol), which manifests that the cellulose will be more favorable to interact with each other in this way. In addition, the number of O—H. . .O type H-bond of A_4 is more than that of A_{2-3}, it

Table 2
The interaction energies $\Delta E_{BSSE+ZPE}$ (kJ/mol) and properties of the electron density of bond critical point for the interaction of Glc–Glc (a.u).

Conformer	Bond	ρ_{BCP}	$\Delta^2\rho_{BCP}$	$\Delta E_{BSSE+ZPE}$
A_2	O2—H. . .O4	0.0319	0.1029	−22.68
A_3	O2—H. . .O6	0.0343	0.1073	−34.57
	O6—H. . .O1	0.0253	0.0835	
A_4	O6—H. . .O1	0.0242	0.0826	−37.93
	O2—H. . .O6	0.0198	0.0698	
	O6—H. . .O3	0.0206	0.0675	

seems that it can account for the interaction energy of A_4 is bigger than that of A_{2-3}.

The intermolecular interaction energies and AIM analysis results of [emim]Ac–Glc are shown in Table 3. It can be found the absolute values of interaction energies of configurations of [emim]Ac–Glc is in an order of $B_3 > B_1 > B_2$. It is clear that [emim]Ac mainly interacts with Glc through the cationic part, the interaction energy is smaller than [emim]Ac mainly interacts with Glc through the anionic part. This implies that the anion plays a major role in the interaction with Glc (Liu, Sale, Holmes, Simmons, & Singh, 2010; Remsing et al., 2008), while the cation probably plays a secondary role. In agreement with the ^{13}C NMR relaxation time data (Remsing et al., 2006), the cations only weakly interact with the sugar. The results are also consistent with the previous reported that the dissolution of cellulose in the ILs should be a result of the joint interactions of anions and cations with cellulose (Guo

Table 3
The interaction energies $\Delta E_{BSSE+ZPE}$ (kJ/mol) and properties of the electron density of bond critical point for the intermolecular interaction of [emim]Ac–Glc (a.u).

Conformer	Bond	ρ_{BCP}	$\Delta^2\rho_{BCP}$	$\Delta E_{BSSE+ZPE}$
B_1	C6—H...O2	0.0059	0.0257	−52.14
	C1—H...O1	0.0136	0.0441	
	C5—H...O1	0.0062	0.0216	
B_2	C1—H...O3	0.0085	0.0310	−10.07
B_3	C2—H...O2	0.0067	0.0248	−93.72
	O2—H...O1	0.0451	0.1474	
	C5—H...O1	0.0048	0.0181	
	C3—H...O3	0.0032	0.0125	

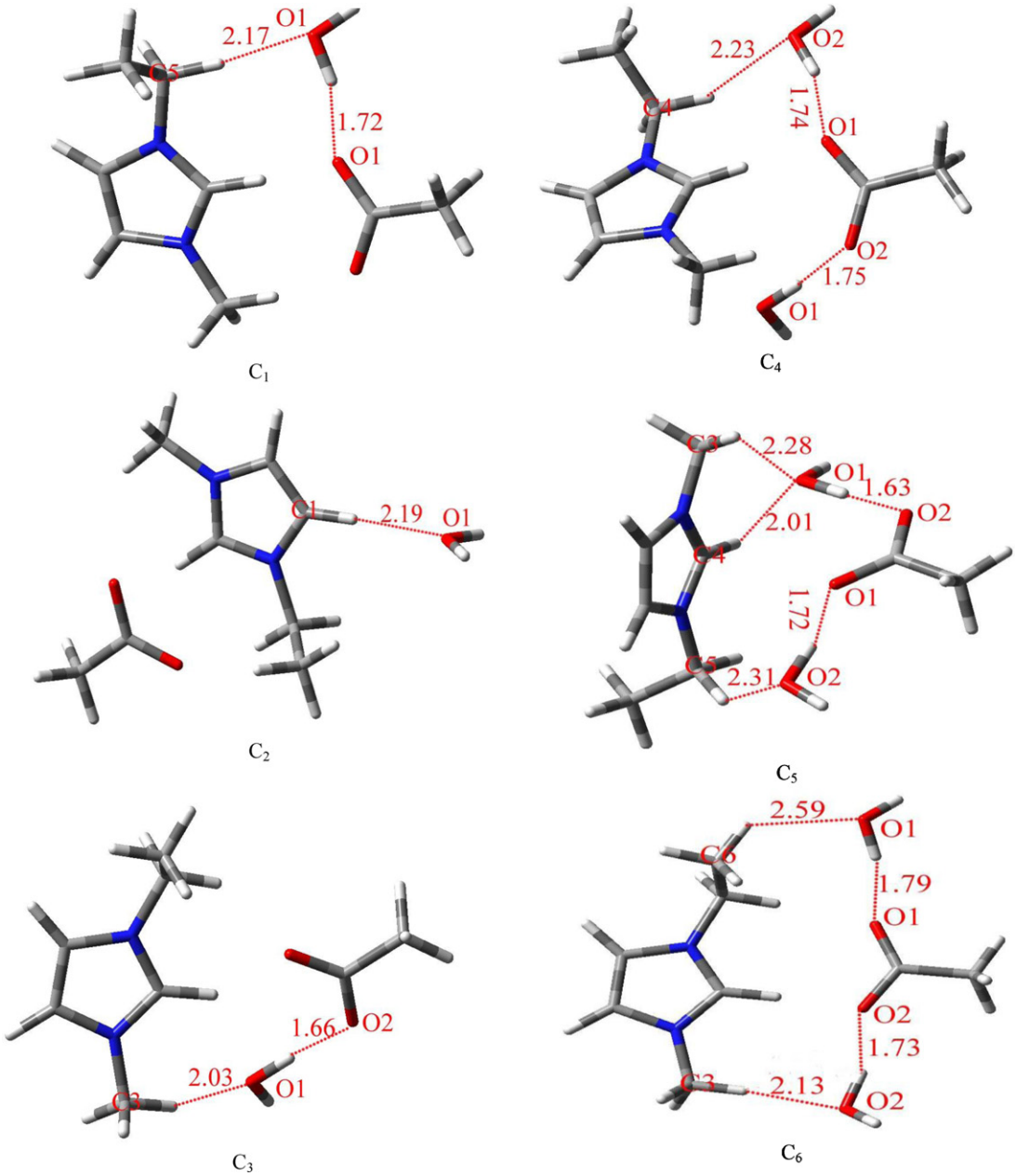

Fig. 2. The optimized configurations for [emim]Ac–nH$_2$O (C_{1-9}; n = 1, 2, 3) calculated at the B3LYP/6-31+G* level. H-bonds are indicated by dotted line, and bond lengths are in angstrom (Å).

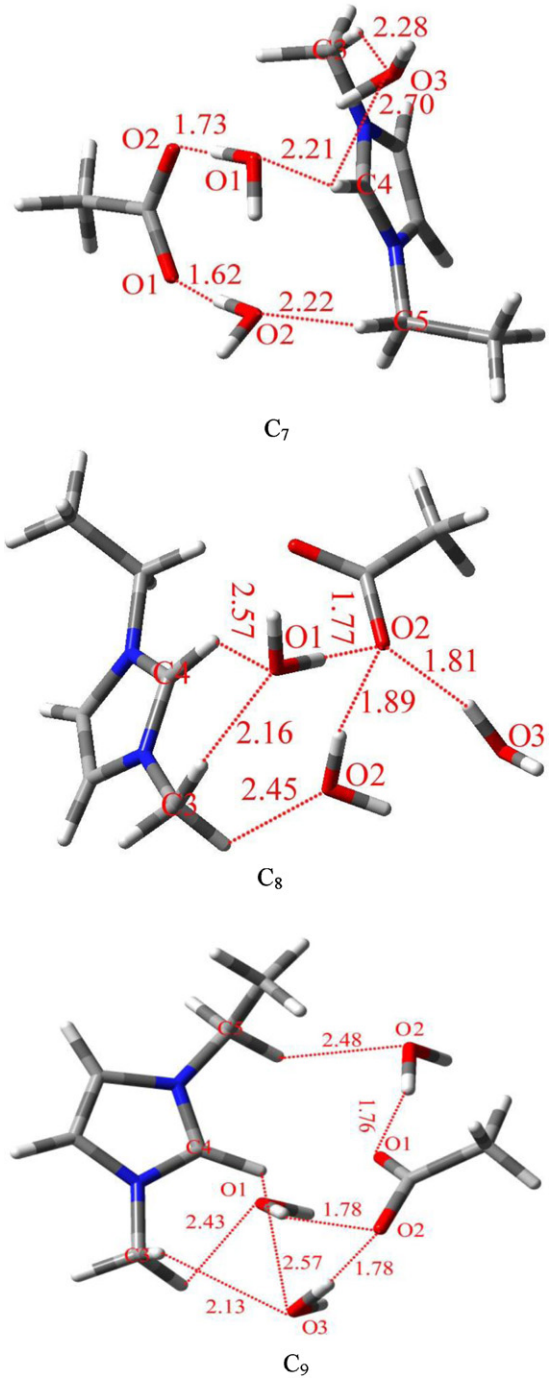

Fig. 2. (*Continued.*)

et al., 2010a; Youngs et al., 2007; Zhang et al., 2005). The absolute values of interaction energies (93.72 and 52.14 kJ/mol) of B_3 and B_1 are bigger than that of Glc–Glc (37.93 kJ/mol). This means that cellulose is easier to combine with [emim]Ac, that is to say [emim]Ac can dissolve cellulose. For all H-bonds considered in this study, the ρ_c and $\nabla^2\rho_c$ values lie in the relative proposed ranges. Therefore, for the observed [emim]Ac–Glc, ρ_c and $\nabla^2\rho_c$ at BCPs of H bonds fall within 0.002–0.050 a.u. and 0.010–0.148 a.u., respectively. It can be concluded that the interactions between [emim]Ac and Glc which are marked by the dotted line are all closed shell system (H-bonds interaction). It was clear that [emim]Ac connects with cellulose by H-bond, which is in agreement with the previous reported conclusion (Swatloski, Spear, Holbrey, & Rogers, 2002). Youngs et al. (2007) also indicted that the dominant contributions to the sugar-ionic liquid interaction energy come from favorable H-bond interactions. This confirmed that [emim]Ac appears to be the most effective solvent, which can dissolve cellulose through H-bonds between hydroxyl functions of cellulose and acetate anions. The results are consistent with the previous reported that the cellulose-acetate anions form strong interaction (Guo et al., 2010b) and glucose–ionic liquid interactions in the liquid are H-bonds between acetate and sugar hydroxyl groups (Youngs et al., 2011).

Most of the ILs can absorb water from the atmosphere (Visser, Swatloski, Reichert, Griffin, & Rogers, 2000), such as [emim]Ac. Water molecules tend to interact with the ILs, this hydrophilic property would sometimes affect their physical properties, the

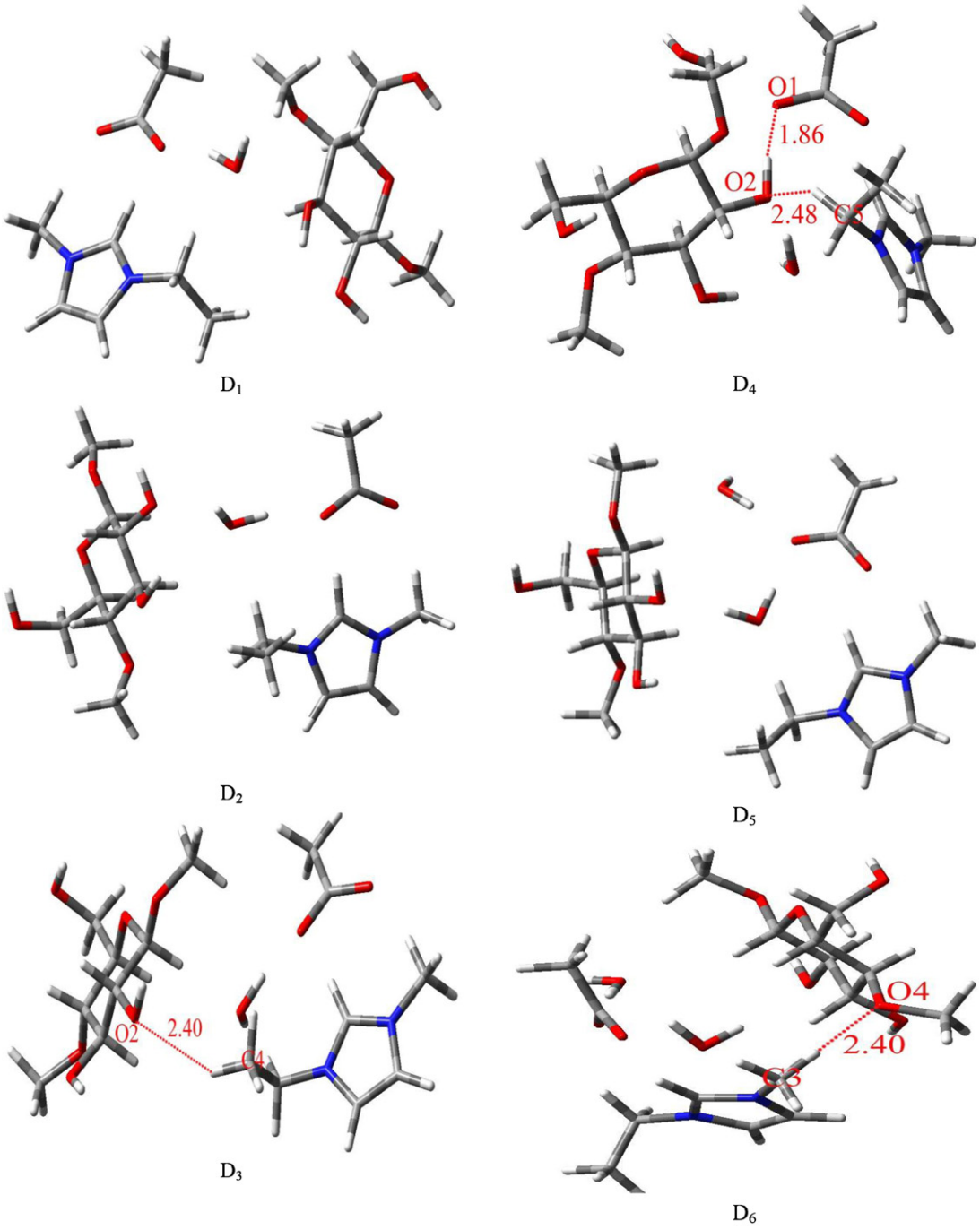

Fig. 3. The optimized configurations for [emim]Ac–Glc–nH$_2$O (D_{1-6}; n = 1, 2) calculated at the B3LYP/6-31+G* level. H-bonds are indicated by dotted line, and bond lengths are in angstrom (Å).

rates and selectivity of reactions (Anthony, Maginn, & Brennecke, 1998; Seddon & Stark, 2002). The quantum chemical (QM) calculations are valuable technique for giving insight at the molecular level into the interactions between water molecules and ILs. For example, Li et al. had applied QM calculations to investigate the interaction between water molecules and ionic liquids based on the imidazolium cation with the anions Cl^-, Br^-, BF_4^-, and PF_6^- (Wang, Li, & Han, 2006). At our QM level, the optimized geometries suggested that there are three types of conformations: [emim]Ac–H_2O, [emim]Ac–$2H_2O$ and [emim]Ac–$3H_2O$. A set of possible conformations of [emim]Ac–nH$_2$O (n = 1, 2, 3) have been examined by DFT calculations to characterize the interactions between H_2O and [emim]Ac. Nine optimized geometries and the interaction energies of [emim]Ac–H_2O are shown in Fig. 2 and Table 4, respectively. It is clear that when one water molecule mainly interacts with the [emim]Ac through the cationic part, using conformation C_2 as reference, the absolute value of interaction energy is 5.24 kJ/mol. However, when water molecule mainly interacts with the [emim]Ac through the anion part, using the complex C_3 as reference, the absolute value of interaction energy is 75.05 kJ/mol. This implies that the anion plays a major role in the interaction of [emim]Ac with water molecule (Cammarata, Kazarian, Salter, & Welton, 2001), while the cation probably play a secondary role. The results are agreement with the previous reported that the strengths of the interactions follow the trend anion–H_2O > cation–H_2O (Wang et al., 2006).

Table 4
The interaction energies $\Delta E_{BSSE+ZPE}$ (kJ/mol) and properties of the electron density of critical point for the intermolecular interaction of [emim] Ac–nH_2O (n = 1, 2, 3; a.u).

Conformer	Bond	ρ_{BCP}	$\Delta^2\rho_{BCP}$	$\Delta E_{BSSE+ZPE}$
C_1	C5—H...O1	0.0172	0.0551	−49.41
	O1—H...O1	0.0413	0.1430	
C_2	C1—H...O1	0.0152	0.0533	−5.24
C_3	C3—H...O1	0.0234	0.0751	−75.05
	O1—H...O2	0.0524	0.1371	
C_4	C4—H...O2	0.0149	0.0499	−94.76
	O2—H...O1	0.0392	0.1262	
	O1—H...O2	0.0382	0.1345	
C_5	C3—H...O1	0.0140	0.0464	−141.54
	C4—H...O1	0.0234	0.0790	
	C5—H...O2	0.0138	0.0458	
	O2—H...O1	0.0428	0.1367	
	O1—H...O2	0.0543	0.1646	
C_6	C6—H...O1	0.0075	0.0281	−86.95
	O1—H...O1	0.0339	0.1208	
	C3—H...O2	0.0182	0.0589	
	O2—H...O2	0.0339	0.1208	
C_7	C4—H...O3	0.0143	0.0467	−170.62
	O2—H...O1	0.0531	0.1639	
	O1—H...O2	0.0407	0.1264	
	C4—H...O1	0.0174	0.0504	
	C5—H...O2	0.0174	0.0504	
	C3—H...O3	0.0161	0.0506	
C_8	O1—H...O2	0.0396	0.1211	−145.42
	O3—H...O2	0.0359	0.1133	
	C3—H...O1	0.0176	0.0584	
	C4—H...O1	0.0082	0.0299	
	C3—H...O2	0.0111	0.0384	
	O2—H...O2	0.0294	0.0922	
C_9	O1—H...O2	0.0386	0.1172	−166.18
	O3—H...O2	0.0356	0.1186	
	O2—H...O1	0.0397	0.1277	
	C5—H...O2	0.0080	0.0339	
	C3—H...O1	0.0112	0.0388	
	C3—H...O3	0.0192	0.0615	
	C4—H...O3	0.0069	0.0259	

About the interaction between two water molecules and [emim]Ac, two water molecules with per pair of ions form a symmetrical structure. The configuration C_5 has the biggest absolute value of interaction energy (141.54 kJ/mol), it is bigger than that of [emim]Ac–Glc (93.72 kJ/mol). When three water molecules interact with the [emim]Ac, the biggest absolute value of interaction energy is 170.62 kJ/mol. It shows that the number of H-bond and the interaction energies between [emim]Ac and water molecules tend to increase due to the introduction of H_2O in [emim]Ac. Moreover, the number of O—H...O type H-bond also tends to increase. It is relatively well known that O—H...O type H-bond is far stronger than the C—H...O type H-bond. When there are two or more water molecules interact with the [emim]Ac, the interaction energies are bigger than that of [emim]Ac–Glc. This implies that [emim]Ac priors to interact with water molecules and results in the precipitation of cellulose. Therefore, the water content is one of the important interference factors for the solubility of cellulose. The AIM results and interaction energies of [emim]Ac–$n$$H_2O$ (n = 1, 2, 3) obtained were shown in Table 4. For all H-bonds considered in this study, the ρ_c and $\nabla^2\rho_c$ values lie in the relative proposed ranges. [emim]Ac prefers to form H-bonds with water molecules, as the concentration of water increases, the number of the H-bonds tends to increase.

In this work, impact of water molecules on [emim]Ac–Glc has also been investigated. [emim]Ac and cellulose can form a solution system through H-bonds with each other. However, the binding sites and the interaction energies of [emim]Ac–Glc will be changed by the addition of water. To investigate this problem, the optimized configuration B_3 of [emim]Ac–Glc was taken as the original free fragments to study the influence of water molecules on the interaction of [emim]Ac–Glc. There are many different ways for water molecules interacting with [emim]Ac–Glc system, and a series of initial geometries were obtained by considering that water molecules were placed near hydroxyl of cellulose. The initial geometries were fully optimized, without imaginary vibrational frequencies and six optimized geometries named D_1–D_6 are obtained as shown in Fig. 3. Subsequently, water molecules were removed from the optimized geometries, then, the intermolecular interaction energies and the AIM analysis were carried out between [emim]Ac and Glc. The results are presented in Table 5. It shows that the addition of water molecules can change the binding site of [emim]Ac and Glc, the geometric configurations would also be changed. As the concentration of water increases, the changes of their conformations become obvious, and the interaction energies of [emim]Ac–Glc tend to decrease. When two water molecules were added into the [emim]Ac–Glc system, the range of the absolute values of interaction energies of [emim]Ac–Glc is from 10.59 to 43.13 kJ/mol, with a decrease about 50–80 kJ/mol. It was observed that the H-bonds between [emim]Ac and Glc are weakened or even destroyed when the water molecules were added to the system, the H-bonds of Glc–Glc connected again, resulting in the precipitation of cellulose (Swatloski et al., 2002). The fact not only implies that [emim]Ac prefers to form H-bonds with water, but also can explain the phenomenon of precipitation of the cellulose when water molecules were added to the [emim]Ac and cellulose system.

Table 5
The interaction energies ΔE_{BSSE} (kJ/mol) and properties of the electron density of bond critical point for the intermolecular interaction of [emim]Ac–Glc–nH_2O (n = 1, 2; a.u).

Conformer	Bond	ρ_{BCP}	$\Delta^2\rho_{BCP}$	ΔE_{BSSE}
D1				−14.28
D2				−24.92
D3	C4—H...O2	0.0069	0.0246	−14.29
D4	O2—H...O1	0.0330	0.1215	−43.13
	C5—H...O2	0.0087	0.0297	
D5				−10.59
D6	C3—H...O4	0.0371	0.0110	−17.33

3.2. Experimental study of original and regenerated cellulose

In order to verify the theoretical calculation results are correct, we designed the related FT-IR, XRD, TGA and SEM experiments.

FT-IR spectra of original and regenerated cellulose obtained are very similar. For the regenerated cellulose, the absorption band of the CH_2 bend vibration at 1367 cm^{-1}, weaken and shifts to a lower wavenumber, compared to the 1379 cm^{-1} peak for the original cellulose. Characteristic for the O—H vibrations of cellulose, a broad vibration band locates in the range of 3350–3450 cm^{-1}. Its shape is broader than that of free hydroxyls, which is believed to be caused by the association of the cellulose chains through H-bonds. The absorption band of the O—H vibration of the original cellulose is 3380 cm^{-1}. In contrast, the band of the O—H vibration of the regenerated cellulose shifted to a higher frequency (3437 cm^{-1}). This is a hint for splitting hydrogen bonds to some extent (Kataoka and Kondo, 1998; Zhang et al., 2005; Zhou et al., 2001). But the spectrum of regeneration cellulose shows new peaks in the range of 2000–2500 cm^{-1}. It can speculate that the chain length might be degraded in the case of dissolutions of cellulose in [emim]Ac. It is highly probable that there is a conversion from cellulose I to cellulose II.

The wide-angle X-ray diffraction curves of original and regenerated cellulose are obtained. Clearly, the diffraction curve of original

cellulose is typical cellulose I structure. It has strong crystalline peaks at 14.98°, 16.56° and 22.68° corresponding to the (1 1 0), (1 1 0), and (0 0 2) planes of crystals, and weak crystalline peaks at 34.56° to the (0 0 4) plane (Oh et al., 2005). However, the diffraction curve of regenerated cellulose is typical cellulose II structure by the presence of the broad crystalline peak at around 12.36° and 20.42° (Cao & Tan, 2005). These results indicate that the transformation from cellulose I to cellulose II after the dissolution and regeneration in [emim]Ac. Compared to the original cellulose, the intensity of diffraction peaks of regenerated cellulose reduces significantly. In other words, the crystallinity of regenerated cellulose is lower than the original cellulose. This phenomenon means that, in the dissolution process, IL rapidly broke intermolecular and intramolecular H-bonds and destroyed the original crystalline form. Moreover, the coagulation process was so transitory that unfavorable to the cellulose crystallization. Similar results had been reported by Zhang et al. (2005).

The thermal decomposition curves of the original and regenerated cellulose were determined using TGA. Neglecting small initial drops in weight occurring near 100 °C due to evaporation of retained moisture, a single pronounced decomposition event followed by slow loss of mass was observed in all cases (Fort et al., 2007). The maximum decomposition rate temperature (T_{max}) is calculated from the TGA traces of the cellulose. For original cellulose, the range of T_{max} value is 320–370 °C, and its residual char yields above 500 °C is about 10 wt%. This range of T_{max} is comparable to the regenerated cellulose from [emim]Ac and reconstitution with deionized water, which the range of T_{max} value is 270–350 °C, and gives a higher char yield (nonvolatile carbonaceous material) on pyrolysis, which is indicated by the high residual masses after the decomposition step (Swatloski et al., 2002). While qualitatively, this shows that the variations in the morphology and degree of polymerization of the celluloses recovered from the IL-based cellulose solution (Calahorra, Cortazar, Eguiazabal, & Guzman, 1989).

SEM images of the morphology of the initial and regenerated cellulose were taken at 2000× magnification. The morphology of the regenerated cellulose is significantly changed compared to the original cellulose, with a conglomerate texture in which cellulose fibers are fused into a relatively more homogeneous macrostructure (Sun et al., 2009; Swatloski et al., 2002).

4. Conclusions

In summary, DFT calculations and AIM theory are proven to be efficient characterization methods to study the mechanism of [emim]Ac dissolving cellulose. The theoretical results showed that [emim]Ac forms strong H-bonds with hydroxyl groups of the cellulose which cause the dissolution of cellulose. Further research suggests that the H-bonds between cellulose and [emim]Ac are weakened or even destroyed with addition of water into [emim]Ac-cellulose system which indicates that water molecules prefer to form H-bonds with [emim]Ac. Consequently the H-bonds between cellulose monomers connected again, and cellulose would precipitate out from the [emim]Ac–cellulose solution. The experimental results also prove that cellulose can be readily reconstituted from the [emim]Ac-based cellulose solution by the addition of water and the crystalline structure of cellulose is converted to cellulose II from cellulose I in original cellulose. The theoretical results agree well with the experimental results.

Acknowledgments

The authors are grateful to the Fundamental Research Funds for the Central Universities (JUSRP211A08) and the National University Student Investigation Program (101029520) for financial support.

Appendix A. Supplementary data

Supplementary data associated with this article can be found, in the online version, at doi:10.1016/j.carbpol.2012.01.080.

References

Anthony, J. L., Maginn, E. J., & Brennecke, J. F. (1998). Solubilities and thermodynamic properties of gases in the ionic liquid 1-*n*-butyl-3-methylimidazolium hexafluorophosphate. *The Journal of Physical Chemistry B*, *106*, 7315–7320.

Bader, R. F. W. (1990). *Atom in molecules: A quantum theory* (22nd ed.). New York: Oxford University Press. (Chapter 22)

Bader, R. F. W. (1998). A bond path: A universal indicator of bonded interactions. *The Journal of Physical Chemistry A*, *102*, 7314–7323.

Berg, R. W., Deetlefs, M., Seddon, K. R., Shim, I., & Thompson, J. M. (2005). Raman and ab initio studies of simple and binary 1-alkyl-3-methylimidazolium ionic liquids. *The Journal of Physical Chemistry B*, *109*, 19018–19025.

Bondi, A. (1964). Van der Waals volumes and radii. *The Journal of Physical Chemistry*, *68*, 441–451.

Calahorra, M. E., Cortazar, M., Eguiazabal, J. I., & Guzman, G. M. (1989). Thermogravimetric analysis of cellulose: Effect of the molecular weight on thermal decomposition. *Journal of Applied Polymer Science*, *37*, 3305–3314.

Cammarata, L., Kazarian, S., Salter, P., & Welton, T. (2001). Molecular states of water in room temperature ionic liquids. *Physical Chemistry Chemical Physics.*, *3*, 5192–5200.

Cao, Y., & Tan, H. M. (2005). Study on crystal structures of enzyme-hydrolyzed cellulosic materials by X-ray diffraction. *Enzyme and Microbial Technology*, *36*(2/3), 314–317.

Ellis, B. (1996). Int Pat, WO 96/18459.

Fort, D., Remsing, R., Swatloski, R., Moyna, P., Moyna, G., & Rogers, R. (2007). Can ionic liquids dissolve wood? Processing and analysis of lignocellulosic materials with 1-*n*-butyl-3- methylimida-zolium chloride. *Green Chemistry*, *9*, 63–69.

Frisch, M. J., Trucks, G. W., Schlegel, H. B., Scuseria, G. E., Robb, M. A., Cheeseman, J. R., et al. (2003). *Gaussian 03*. Pittsburgh, PA: Gaussian Inc.

Fu, D., Mazza, G., & Tamaki, Y. J. (2010). Lignin extraction from straw by ionic liquids and enzymatic hydrolysis of the cellulosic residues. *Journal of Agricultural Food Chemistry*, *58*, 2915–2922.

Guo, J., Zhang, D., Duan, C., & Liu, C. (2010). Probing anion–cellulose interactions in imidazolium-based room temperature ionic liquids: A density functional study. *Carbohydrate Research*, *345*, 2201–2205.

Guo, J., Zhang, D., & Liu, C. (2010). A theoretical investigation of the interactions between cellulose and 1-butyl-3-methylimidazolium chloride. *Journal of Theoretical and Computational Chemistry*, *9*, 611–624.

Huddleston, J. G., Visser, A. E., Reichert, W. M., Willauer, H. D., Broker, G. A., & Rogers, R. D. (2001). Characterization and comparison of hydrophilic and hydrophobic room temperature ionic liquids incorporating the imidazolium cation. *Green Chemistry*, *3*, 156–164.

Janesko, B. G. (2011). Modeling interactions between lignocellulose and ionic liquids using DFT-D. *Physical Chemistry Chemical Physics*, *13*, 11393–11401.

Johnson, D. C., Nevell, T. P., & Zeronian, S. H. (1985). *Cellulose chemistry and its application* (181). Chichester: E. Horwood. (Chapter 181).

Kataoka, Y., & Kondo, T. (1998). FT-IR microscopic analysis of changing cellulose crystalline structure during wood cell wall formation. *Macromolecules*, *31*, 760–764.

Kirk-Othmer. (1993). *Encyclopedia of chemical technology* (4th ed.). New York: Wiley. (Chapter 4).

Lee, C., Yang, W., & Parr, R. G. (1988). Development of the Colle–Salvetti correlation-energy formula into a functional of the electron density. *Physical Review B*, *37*, 785–789.

Li, C., & Zhao, Z. (2007). Efficient acid-catalyzed hydrolysis of cellulose in ionic liquid. *Advanced Synthesis & Catalysis*, *349*, 1847–1850.

Liu, H., Sale, K. L., Holmes, B. M., Simmons, B. A., & Singh, S. (2010). Understanding the interactions of cellulose with ionic liquids: A molecular dynamics study. *The Journal of Physical Chemistry B*, *114*, 4293–4301.

Oh, S. Y., Yoo, D. I., Shin, Y., Kim, H. C., Kim, H. Y., Chung, Y. S., et al. (2005). Crystalline structure analysis of cellulose treated with sodium hydroxide and carbon dioxide by means of X-ray diffraction and FTIR spectroscopy. *Carbohydrate Research*, *340*, 2376–2391.

Parr, R. G., & Yang, W. (1994). *Density-functional theory of atoms and molecules* (16th ed.). Oxford: Oxford Science. (Chapter 16).

Remsing, R. C., Hernandez, G., Swatloski, R. P., Massefski, W. W., Rogers, R. D., & Moyna, G. (2008). Solvation of carbohydrates in *N*,*N*′-dialkylimidazolium ionic liquids: A multinuclear NMR spectroscopy study. *The Journal of Physical Chemistry B*, *112*, 11071–11078.

Remsing, R. C., Swatloski, R. P., Rogers, R. D., & Moyna, G. (2006). Mechanism of cellulose dissolution in the ionic liquid 1-*n*-butyl-3-methylimidazolium chloride: A ^{13}C and $^{35/37}Cl$ NMR relaxation study on model systems. *Chemical Communications*, *12*, 1271–1273.

Seddon, K. R., & Stark, A. (2002). Selective catalytic oxidation of benzyl alcohol and alkylbenzenes in ionic liquids. *Green Chemistry*, *4*, 119–123.

Solimannejad, M., Alkorta, I., & Elguero, J. (2007). Stabilities and properties of O_3–HOCl complexes: A computational study. *Chemical Physics Letters*, *449*, 23–27.

Song, Z., Wang, H., & Xing, L. (2009). Density functional theory study of the ionic liquid [emim]OH and complexes [emim]OH $(H_2O)_n$ ($n = 1, 2$). *Journal of Solution Chemistry*, *38*, 1139–1154.

Sun, N., Rahman, M., Qin, Y., Maxim, M., Rodriguez, H., & Rogers, R. (2009). Complete dissolution and partial delignification of wood in the ionic liquid 1-ethyl-3-methylimidazolium acetate. *Green Chemistry*, *11*, 646–655.

Swatloski, R., Spear, S., Holbrey, J., & Rogers, R. (2002). Dissolution of cellulose with ionic liquids. *Journal of American Chemical Society*, *124*, 4974–4975.

Tan, S. S. Y., MacFarlane, D. R., Upfal, J., Edye, L. A., Doherty, W. O. S., Patti, A. F., et al. (2009). Extraction of lignin from lignocellulose at atmospheric pressure using alkylbenzenesulfonate ionic liquid. *Green Chemistry*, *11*, 339–345.

Visser, A. E., Swatloski, R. P., Reichert, W. M., Griffin, S. T., & Rogers, R. D. (2000). Traditional extractants in nontraditional solvents: Groups 1 and 2 extraction by crown ethers in room-temperature ionic liquids. *Industrial & Engineering Chemistry Research*, *39*, 3596–3604.

Wang, Y., Li, H., & Han, S. (2006). A theoretical investigation of the interactions between water molecules and ionic liquids. *The Journal of Physical Chemistry B*, *110*, 24646–24651.

Yang, J. Z., Zhang, Q. G., Wang, B., & Tong, J. (2006). A theoretical investigation of the interactions between water molecules and ionic liquids. *The Journal of Physical Chemistry B*, *110*, 22521–22524.

Youngs, T., Hardacre, C., & Holbrey, J. (2007). Glccose solvation by the ionic liquid 1, 3-dimethylimidazolium chloride: A simulation study. *The Journal of Physical Chemistry B*, *111*, 13765–13774.

Youngs, T. G. A., Holbrey, J. D., Mullan, C. L., Norman, S. E., Lagunas, M. C., D'Agostino, C., et al. (2011). Neutron diffraction, NMR and molecular dynamics study of glucose dissolved in the ionic liquid 1-ethyl-3-methylimidazolium acetate. *The Royal Society of Chemistry*, *2*, 1594–1605.

Zhang, H., Wu, J., Zhang, J., & He, J. (2005). 1-Allyl-3-methylimidazolium chloride room temperature ionic liquid: A new and powerful nonderivatizing solvent for cellulose. *Macromolecules*, *38*, 8272–8277.

Zhou, S. M., Tashiro, K., Hongo, T., Shirataki, H., Yamane, C., & Ii, T. (2001). Influence of water on structure and mechanical properties of regenerated cellulose studied by an organized combination of infrared spectra, X-ray diffraction and dynamic viscoelastic data measured as functions of temperature and humidity. *Macromolecules*, *34*, 1274–1280.